Triton with long-range chiral N^{3}LO three-nucleon forces

R. Skibiński,[1] J. Golak,[1] K. Topolnicki,[1] H. Witała,[1] E. Epelbaum,[2] W. Glöckle,[2] H. Krebs,[2] A. Nogga,[3,*] and H. Kamada[4]

[1]*M. Smoluchowski Institute of Physics, Jagiellonian University, PL-30059 Kraków, Poland*

[2]*Institut für Theoretische Physik II, Ruhr-Universität Bochum, D-44780 Bochum, Germany*

[3]*Forschungszentrum Jülich, Institut für Kernphysik, Institute for Advanced Simulation and Jülich Center for Hadron Physics, D-52425 Jülich, Germany*

[4]*Department of Physics, Faculty of Engineering, Kyushu Institute of Technology, Kitakyushu 804-8550, Japan*

(Received 27 July 2011; revised manuscript received 6 October 2011; published 15 November 2011)

Long-range contributions to the three-nucleon force that have recently been worked out in chiral effective-field theory at next-to-next-to-next-to-leading order are, for the first time, included in the triton and the doublet nucleon-deuteron scattering length calculations. The strengths of the two short-range terms available at this order in the chiral expansion are determined from the triton binding energy and the neutron-deuteron doublet scattering length. The structure of the resulting three-nucleon force is explored and effects for the two-nucleon correlation function in the triton are investigated. Expectation values of the individual contributions to the three-nucleon force in the triton are found to be in the range of a few hundred kilo–electron volts to about 1 MeV. Our study demonstrates that the very complicated operator structure of the novel chiral three-nucleon forces can be successively implemented in three-nucleon Faddeev calculations.

DOI: 10.1103/PhysRevC.84.054005 PACS number(s): 21.30.Fe, 21.45.Ff

I. INTRODUCTION

Chiral effective-field theory (EFT) provides a powerful framework for the systematical description of low-energy dynamics of few- and many-nucleon systems. Various variants of effective theories for nuclear forces have been explored; see Refs. [1–3] for recent review articles. Up to now, the most advanced few-nucleon studies have been carried out within a framework based on pions and nucleons as the only explicit degrees of freedom taken into account in the effective Lagrangian. Within this approach, the nucleon-nucleon (NN) force is currently available up to next-to-next-to-next-to-leading order (N^{3}LO) in the chiral expansion. At this chiral order, it receives contributions from one-, two-, and three-pion exchange diagrams as well as short-range NN contact interactions with up to four derivatives. As demonstrated in Refs. [4] and [5], NN phase shifts are accurately described at N^{3}LO up to laboratory energies of the order of 200 MeV. The theoretical uncertainty owing to truncation of the chiral expansion is estimated in Ref. [4] by means of a cutoff variation. Within the spectral function regularization (SFR) framework [6] adopted in Ref. [4], the NN potential depends on two ultraviolet cutoffs, $\tilde{\Lambda}$ and Λ. The first one removes large-mass components in the spectrum of the two-pion exchange potential that cannot be correctly described within the chiral EFT framework, while the other one provides regularization of the Lippmann-Schwinger equation. Five combinations of these cutoff parameters are available for the NN potentials in Ref. [4]. The residual dependence of low-energy observables on the cutoff choice provides a measure of the importance of higher-order contact interactions and thus may serve as an estimate of the theoretical uncertainty.

Parallel to these developments three-nucleon force (3NF) has also been explored within the framework of chiral EFT. The first nonvanishing contributions to the 3NF emerge at next-to-next-to-leading order (N^{2}LO) [7] from the two-pion exchange and one-pion exchange-contact diagrams as well as the purely short-range derivativeless three-nucleon contact interaction [7] (see also Ref. [8] for a pioneering work along this line). The resulting N^{2}LO three-nucleon potential depends on two low-energy constants (LECs), D and E, accompanying the short-range πNN and NNN vertices, respectively. The values of these LECs need to be fixed from a fit to few-nucleon data. Among the few possible observables that have been used in this connection are the triton binding energy and the nucleon-deuteron doublet scattering length $^2a_{nd}$ [7,9], the α-particle binding energy [10,11], the properties of light nuclei [12], and the triton β decay [13]. The N^{2}LO 3NF from Ref. [7] was successfully used in three-body calculations (see Refs. [14] and [15] for a few examples of recent studies). At this order, the chiral EFT yields a good description of elastic scattering and deuteron breakup observables up to energies of about ≈50 MeV. The accuracy of the results in this regime is comparable with the accuracy achieved by realistic phenomenological NN and 3N interactions such as, e.g., AV18 [16] 2NF in combination with UrbanaIX [17] 3NF or CD-Bonn [18] 2NF in combination with the Tucson-Melbourne [19] 3NF (see Refs. [14] and [20]). However, the spread of the results is relatively large for some spin observables, which clearly calls for the inclusion of new terms of the nuclear interaction that occur at higher orders of the chiral expansion.

Subleading contributions to the 3NF are currently being investigated by several groups. At N^{3}LO, one has to take into account (irreducible) contributions emerging from all possible one-loop, three-nucleon diagrams constructed with the lowest order vertices. In addition, there are (tree-level) leading relativistic corrections; see Ref. [21] for an early work on the longest range relativistic corrections. Note that tree

*a.nogga@fz-juelich.de

diagrams involving higher-order vertices from the effective chiral Lagrangian do not produce any irreducible pieces. Effects owing to two-pion exchange 3NF in elastic nucleon-deuteron scattering were already explored by Ishikawa and Robilotta [22] within a hybrid approach and found to be rather small. The N^{3}LO contributions feed into five topologies, as explained in detail in the next section. The explicit expressions both in momentum and in coordinate space for long-range contributions have already been worked out [22,23]. Their inclusion in numerical few-body calculations appears to be challenging owing to the very rich and complicated operator structure. The large number of terms in the 3NF at N^{3}LO (see Ref. [23]) requires an efficient method of performing partial-wave decomposition. Recently such a method was proposed [24] and tested for the Tucson-Melbourne force [25]. Here and in what follows, this approach is referred to as the automatized partial-wave decomposition (aPWD). In this paper we apply this method of numerical partial-wave decomposition to the N^{3}LO3 NF contributions derived in Ref. [23]. For the first time, the parts of 3NF at N^{3}LO different from the two-pion exchange force are included in the triton and the scattering length calculations. In order to test the implementations and get a first hint as to the possible effects of these forces, we fix the two LECs entering the 3NF from the triton binding energy and the nucleon-deuteron doublet scattering length and explore the effects owing to these novel 3NF terms by computing the ^{3}H properties. Although this calculations is still incomplete, as not all 3NF contributions at N^{3}LO are taken into account, it provides an important first step toward the complete N^{3}LO analysis of 3N scattering and demonstrates our ability to numerically handle the rather complicated structure of the subleading chiral 3NF.

Our paper is organized as follows. In Sec. II we briefly describe the structure of the chiral 3NF at N^{3}LO. In Sec. III we discuss in detail the partial-wave decomposition needed in our scattering and bound-state calculations. Next, the procedure for fixing the LECs is described in Sec. IV, where the obtained values of LECs are also listed. These results are used in Sec. V to explore some properties of the triton. Finally, our findings are summarized in Sec. VI.

II. 3NF AT N^{3}LO

The subleading (i.e., N^{3}LO) contributions to the 3NF V_{123} can be written in the form [23]

$$V_{123} = V_{2\pi} + V_{2\pi\text{-}1\pi} + V_{\text{ring}} + V_{1\pi\ \text{cont}} + V_{2\pi\ \text{cont}} + V_{1/m}, \tag{2.1}$$

where the individual terms refer, in order, to the two-pion exchange, two-pion/one-pion exchange, ring (i.e. one pion being exchanged between each of the three nucleon pairs), one-pion exchange-contact, and two-pion exchange-contact contributions as well as the leading relativistic corrections (see Fig. 1 in Ref. [23] for a diagrammatic representation). The expressions for the (static) long-range part of the 3NF given by the first three terms in the above equation were worked out in heavy-baryon chiral perturbation theory in Ref. [23]. The two-pion exchange contribution at the one-loop level was also calculated within the infrared-regularized version of chiral perturbation theory in Ref. [22]. The shorter range contributions involving two-nucleon contact interactions and relativistic corrections are currently being worked out [26].

While the two-pion exchange $V_{2\pi}$ and one-pion exchange-contact parts $V_{1\pi\ \text{cont}}$ already occur at N^{2}LO and receive corrections at N^{3}LO, the remaining topologies first emerge at N^{3}LO. It is important to emphasize that all subleading contributions to the 3NF are parameter-free. Thus, the LECs D and E entering the one-pion exchange-contact and the purely short-range parts of the 3NF at N^{2}LO are the only unknown parameters up to N^{3}LO.

Here and in what follows, we adopt the notation in which a given 3NF V_{123} is decomposed into three terms,

$$V_{123} = V^{(1)} + V^{(2)} + V^{(3)}, \tag{2.2}$$

where each $V^{(i)}$ is symmetrical under interchanging nucleons j and k ($i, j, k = 1, 2, 3$, $i \neq j \neq k$). Clearly, this condition does not specify $V^{(1)}$ uniquely. In the following we choose $V^{(1)}$ in such a way that the number of operator structures is minimized, which is convenient for the aPWD.

The operator structure of the 2π exchange part $V_{2\pi}^{(1)}$ at N^{3}LO remains the same as at N^{2}LO,

$$V_{2\pi}^{(1)} = F_1 \vec{\sigma}_2 \cdot \vec{q}_2 \vec{\sigma}_3 \cdot \vec{q}_3 \boldsymbol{\tau}_2 \cdot \boldsymbol{\tau}_3 + F_2 \vec{\sigma}_2 \cdot \vec{q}_2 \vec{\sigma}_3 \cdot \vec{q}_3 \vec{q}_2 \times \vec{q}_3 \cdot \vec{\sigma}_1 \boldsymbol{\tau}_2 \times \boldsymbol{\tau}_3 \cdot \boldsymbol{\tau}_1, \tag{2.3}$$

where $\vec{q}_i$ is the momentum transfer to the ith nucleon, and $\vec{q}_1 + \vec{q}_2 + \vec{q}_3 = 0$ and $\vec{\sigma}_i$ ($\boldsymbol{\tau}_i$) are Pauli spin (isospin) matrices for nucleon i. The scalar functions $F_1 = F_1(q_2, q_3, \hat{q}_2 \cdot \hat{q}_3)$ and $F_2 = F_2(q_2, q_3, \hat{q}_2 \cdot \hat{q}_3)$ depend on the LECs $\tilde{c}_{1,3,4}$, which accompany the subleading pion-nucleon vertices. Chiral expansion of F_1 and F_2 up to N^{3}LO has the form [23]

$$F_1 = \frac{g_A^4}{4F_\pi^4} \frac{(-4\tilde{c}_1 M_\pi^2 + 2\tilde{c}_3 \vec{q}_2 \cdot \vec{q}_3)}{(q_2^2 + M_\pi^2)(q_3^2 + M_\pi^2)} + \tilde{F}_1, \tag{2.4}$$

$$F_2 = \frac{g_A^4}{4F_\pi^4} \frac{\tilde{c}_4}{(q_2^2 + M_\pi^2)(q_3^2 + M_\pi^2)} + \tilde{F}_2, \tag{2.5}$$

with

$$\tilde{F}_1 = \frac{g_A^4}{128\pi F_\pi^6} \frac{1}{(q_2^2 + M_\pi^2)(q_3^2 + M_\pi^2)} \Big(M_\pi (M_\pi^2 + 3q_2^2 + 3q_3^2 + 4\vec{q}_2 \cdot \vec{q}_3) + (2M_\pi^2 + q_2^2 + q_3^2 + 2\vec{q}_2 \cdot \vec{q}_3)(3M_\pi^2 + 3q_2^2 + 3q_3^2 + 4\vec{q}_2 \cdot \vec{q}_3) A(|\vec{q}_2 + \vec{q}_3|) \Big), \tag{2.6}$$

$$\tilde{F}_2 = \frac{-g_A^4}{128\pi F_\pi^6} \frac{1}{(q_2^2 + M_\pi^2)(q_3^2 + M_\pi^2)} \Big(M_\pi + (4M_\pi^2 + q_2^2 + q_3^2 + 2\vec{q}_2 \cdot \vec{q}_3) A(|\vec{q}_2 + \vec{q}_3|) \Big), \tag{2.7}$$

where the loop function $A(q)$ is defined as

$$A(q) = \frac{1}{2q} \arctan \frac{q}{2M_\pi}. \tag{2.8}$$

The axial-vector coupling constant, the weak pion decay constant, and the pion mass are denoted g_A, F_π, and M_π, respectively. Note that the SFR changes $A(q)$ (see Ref. [6]). For the study here we do not need to consider this change, as they differ only by higher order polynomials [1]. The quantities $\tilde{c}_i$ appearing in the above expressions are related to the N^{2}LO LECs c_i entering the effective chiral Lagrangian via

$$\tilde{c}_1 = c_1 - \frac{g_A^2 M_\pi}{64\pi F_\pi^2} = -0.94 \text{ GeV}^{-1},$$

$$\tilde{c}_3 = c_3 + \frac{g_A^4 M_\pi}{16\pi F_\pi^2} = -2.51 \text{ GeV}^{-1},$$

$$\tilde{c}_4 = c_4 - \frac{g_A^4 M_\pi}{16\pi F_\pi^2} = 2.51 \text{ GeV}^{-1},$$

where we have adopted the values for the c_i from Ref. [4], namely,

$$c_1 = -0.81 \text{ GeV}^{-1}, \quad c_3 = -3.40 \text{ GeV}^{-1}, \quad c_4 = 3.40 \text{ GeV}^{-1}. \tag{2.9}$$

These values are consistent with those determined from pion-nucleon scattering [27]. The finite shifts of the LECs c_i in Eq. (2.9) emerge from pion loops at N^{3}LO.

The $V^{(1)}_{2\pi\text{-}1\pi}$ interaction at N^{3}LO has the operator structure

$$V^{(1)}_{2\pi\text{-}1\pi} = \frac{\vec{\sigma}_1 \cdot \vec{q}_1}{q_1^2 + M_\pi^2} [\boldsymbol{\tau}_2 \cdot \boldsymbol{\tau}_1 (\vec{\sigma}_3 \cdot \vec{q}_2 \vec{q}_2 \cdot \vec{q}_1 F_1(q_2) + \vec{\sigma}_3 \cdot \vec{q}_2 F_2(q_2) + \vec{\sigma}_3 \cdot \vec{q}_1 F_3(q_2)) + \boldsymbol{\tau}_3 \cdot \boldsymbol{\tau}_1 (\vec{\sigma}_2 \cdot \vec{q}_2 \vec{q}_2 \cdot \vec{q}_1 F_4(q_2) + \vec{\sigma}_2 \cdot \vec{q} F_5(q_2) + \vec{\sigma}_3 \cdot \vec{q} F_6(q_2) + \vec{\sigma}_3 \cdot \vec{q} F_7(q_2)) + \boldsymbol{\tau}_2 \times \boldsymbol{\tau}_3 \cdot \boldsymbol{\tau}_1 \, \vec{\sigma}_2 \times \vec{\sigma}_3 \cdot \vec{q} F_8(q_2)] + (2 \leftrightarrow 3), \tag{2.10}$$

with scalar functions $F_i(q_i)$. The interchange of nucleons $(2 \leftrightarrow 3)$ refers to the interchange of momentum vectors, spin and isospin matrices, and arguments of the functions F_i. Explicit expressions for the scalar functions $F_i(q_i)$ that appear in the $V^{(1)}_{2\pi\text{-}1\pi}$ can be found in Ref. [23].

The $V^{(1)}_{\text{ring}}$ force is chosen as

$$\begin{aligned} V^{(1)}_{\text{ring}} = {} & \vec{\sigma}_1 \cdot \vec{\sigma}_2 \boldsymbol{\tau}_2 \cdot \boldsymbol{\tau}_3 R_1 + \vec{\sigma}_1 \cdot \vec{q}_1 \vec{\sigma}_2 \cdot \vec{q}_1 \boldsymbol{\tau}_2 \cdot \boldsymbol{\tau}_3 R_2 + \vec{\sigma}_1 \cdot \vec{q}_1 \vec{\sigma}_2 \cdot \vec{q}_3 \boldsymbol{\tau}_2 \cdot \boldsymbol{\tau}_3 R_3 \\ & + \vec{\sigma}_1 \cdot \vec{q}_3 \vec{\sigma}_2 \cdot \vec{q}_1 \boldsymbol{\tau}_2 \cdot \boldsymbol{\tau}_3 R_4 + \vec{\sigma}_1 \cdot \vec{q}_3 \vec{\sigma}_2 \cdot \vec{q}_3 \boldsymbol{\tau}_2 \cdot \boldsymbol{\tau}_3 R_5 + \boldsymbol{\tau}_1 \cdot \boldsymbol{\tau}_3 R_6 + \vec{\sigma}_1 \cdot \vec{q}_1 \vec{\sigma}_3 \cdot \vec{q}_1 R_7 \\ & + \vec{\sigma}_1 \cdot \vec{q}_1 \vec{\sigma}_3 \cdot \vec{q}_3 R_8 + \vec{\sigma}_1 \cdot \vec{q}_3 \vec{\sigma}_3 \cdot \vec{q}_1 R_9 + \vec{\sigma}_1 \cdot \vec{\sigma}_3 R_{10} + \vec{q}_1 \cdot \vec{q}_3 \times \vec{\sigma}_2 \boldsymbol{\tau}_1 \cdot \boldsymbol{\tau}_2 \times \boldsymbol{\tau}_3 R_{11} \\ & + \boldsymbol{\tau}_1 \cdot \boldsymbol{\tau}_2 S_1 + \vec{\sigma}_1 \cdot \vec{q}_1 \vec{\sigma}_3 \cdot \vec{q}_1 \boldsymbol{\tau}_1 \cdot \boldsymbol{\tau}_2 S_2 + \vec{\sigma}_1 \cdot \vec{q}_3 \vec{\sigma}_3 \cdot \vec{q}_1 \boldsymbol{\tau}_1 \cdot \boldsymbol{\tau}_2 S_3 + \vec{\sigma}_1 \cdot \vec{q}_1 \vec{\sigma}_3 \cdot \vec{q}_3 \boldsymbol{\tau}_1 \cdot \boldsymbol{\tau}_2 S_4 \\ & + \vec{\sigma}_1 \cdot \vec{q}_3 \vec{\sigma}_3 \cdot \vec{q}_3 \boldsymbol{\tau}_1 \cdot \boldsymbol{\tau}_2 S_5 + \vec{\sigma}_1 \cdot \vec{\sigma}_3 \boldsymbol{\tau}_1 \cdot \boldsymbol{\tau}_2 S_6 + \vec{q}_1 \cdot \vec{q}_3 \times \vec{\sigma}_1 \boldsymbol{\tau}_1 \cdot \boldsymbol{\tau}_2 \times \boldsymbol{\tau}_3 S_7 + (2 \leftrightarrow 3), \end{aligned} \tag{2.11}$$

where the expressions for the scalar functions $R_i = R_i(q_1, q_3, \hat{q}_1 \cdot \hat{q}_3)$ and $S_i = S_i(q_1, q_3, \hat{q}_1 \cdot \hat{q}_3)$ are given in Ref. [23].

Modifications of the one-pion exchange-contact $V^{(1)}_{1\pi \text{ cont}}$ term arising at N^{3}LOare in preparation [26]. Thus, instead of the full $V^{(1)}_{1\pi-\text{cont}}$ interaction we use the lowest order result for it, resulting in N^{2}LO [7]:

$$V^{(1)}_{d \text{ term}} = -\frac{g_A D}{8F_\pi^2} \frac{\vec{\sigma}_1 \cdot \vec{q}_1}{q_1^2 + M_\pi^2} (\boldsymbol{\tau}_1 \cdot \boldsymbol{\tau}_3 \vec{\sigma}_3 \cdot \vec{q}_1 + \boldsymbol{\tau}_1 \cdot \boldsymbol{\tau}_2 \vec{\sigma}_2 \cdot \vec{q}_1). \tag{2.12}$$

The LEC D can be expressed as $D = c_D/(F_\pi^2 \Lambda_\chi)$, where c_D is a dimensionless free parameter and the chiral symmetry breaking scale Λ_χ is estimated to be $\Lambda_\chi = 700$ MeV. Here and in what follows, we use $F_\pi = 92.4$ MeV for the pion decay constant. The value of c_D has to be determined from experimental data. This is described in Sec. IV for our fit for the test case in this study. Of course, the results of this fit will significantly change when the complete short-range interaction is taken into account.

As already pointed out, the remaining terms $V^{(1)}_{2\pi \text{ cont}}$ and $V^{(1)}_{1/m}$ are also not available yet [26] and thus cannot be taken into account in the present study. Finally, the purely short-range part of the 3NF has the form [7]

$$V^{(1)}_{e \text{ term}} = E \boldsymbol{\tau}_2 \cdot \boldsymbol{\tau}_3. \tag{2.13}$$

Again, the LEC E is usually expressed in terms of a dimensionless parameter c_E via $E = c_E/(F_\pi^4 \Lambda_\chi)$, which needs to be determined from (at least) three-nucleon data.

To summarize, in this paper we use the $V^{(1)}_{2\pi}$, $V^{(1)}_{2\pi\text{-}1\pi}$, and $V^{(1)}_{\text{ring}}$ N^{3}LO terms combined with the $V^{(1)}_{d \text{ term}}$ and $V^{(1)}_{e \text{ term}}$ terms at N^{2}LO. The N^{3}LO contributions to $V^{(1)}_{1\pi \text{ cont}}$ and $V^{(1)}_{2\pi \text{ cont}}$ and relativistic corrections $V^{(1)}_{1/m}$ are not included. Finally, the remaining terms $V^{(2)}$ and $V^{(3)}$ of Eq. (2.2) can be obtained from $V^{(1)}$ by appropriate permutations of nucleons.

III. NUMERICAL CALCULATIONS OF 3NF MATRIX ELEMENTS

We work in the momentum space using three-nucleon partial-wave states $|p, q, \alpha\rangle$ in the jJ coupling [28,29]

$$|p, q, \alpha\rangle \equiv \left|pq(ls)j\left(\lambda \tfrac{1}{2}\right)I(jI)JM_J\right\rangle \left|\left(t \tfrac{1}{2}\right)TM_T\right\rangle, \tag{3.1}$$

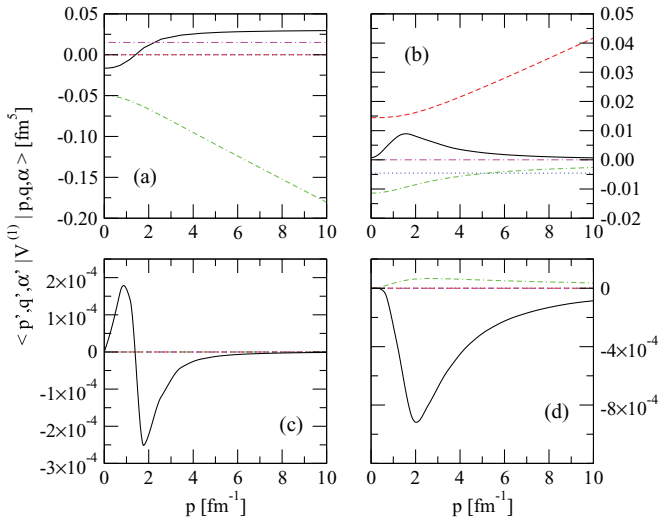

FIG. 1. (Color online) N^{3}LO 3NF matrix elements (before regularization) $\langle p', q', \alpha' | V^{(1)} | p, q, \alpha \rangle$ as a function of the momentum p for $p' = 0.268$ fm, $^{-1}$, $q' = 2.842$ fm^{-1}, and $q = 0.132$ fm^{-1} and different combinations (α', α): (a) (1,1), (b) (1,5), (c) (4,4), and (d) (4,7). Solid (black), dashed (red), double-dash-dotted (green), dotted (blue), and dash-dotted (magenta) lines show the $V_{2\pi}$, $V_{2\pi\text{-}1\pi}$, V_{ring}, $V_{d\ \text{term}}$ and $V_{e\ \text{term}}$ components, respectively.

where p and q are magnitudes of the standard Jacobi momenta and α denotes a set of discrete quantum numbers defined in the following way: the spin s of the subsystem composed of nucleons 2 and 3 is coupled with their orbital angular momentum l to the total angular momentum j. The spin $1/2$ of the spectator particle 1 couples with its relative orbital angular momentum λ to the total angular momentum I of nucleon 1. Finally, j and I are coupled to the total 3N angular momentum J with projection M_J. For the isospin part, the total isospin t of subsystem (23) is coupled with the isospin $1/2$ of the spectator nucleon to the total 3N isospin T with projection M_T.

The matrix elements of $V^{(1)}_{2\pi}$, $V^{(1)}_{2\pi\text{-}1\pi}$, and $V^{(1)}_{\text{ring}}$ forces in the basis $|p, q, \alpha\rangle$ are obtained using the recently proposed aPWD method [24,25]. In this approach the spin-momentum and isospin parts of three-nucleon interactions are calculated using a software for symbolic calculations. The resulting momentum-dependent functions are then integrated numerically in five dimensions over angular variables. The major advantage of this method is its generality. It can be applied to *any* momentum-spin-isospin operator including, in particular, the full operator structure of the 3NF at N^{3}LO, including even the nonlocal relativistic corrections. The only complication emerges in the treatment of the ring contributions to the 3NF owing to rather complex expressions for the functions $R_i = R_i(q_1, q_3, \hat{q}_1 \cdot \hat{q}_3)$ and $S_i = S_i(q_1, q_3, \hat{q}_1 \cdot \hat{q}_3)$, which involve certain scalar integrals related to the three-point function. For any given values of the arguments, these integrals have to be computed numerically. This evaluation is too expensive to be carried out on-the-fly during the aPWD. Moreover, while the functions R_i and S_i are, of course, finite and smooth for all possible values of their arguments, they are given in Ref. [23] as linear combinations of terms, some of which are becoming singular under certain kinematical conditions. Their numerical implementation therefore requires special care. In order to deal with these difficulties, we first evaluate the functions R_i and S_i at a (fixed) dense grid of points for their arguments and then use interpolation to compute them for arbitrary values of q_1, q_3, and $\hat{q}_1 \cdot \hat{q}_3$ as needed in the aPWD approach. We have carefully checked the stability of this procedure by increasing the density of the grid points. Finally, the partial-wave decomposition of $V^{(1)}_{d\ \text{term}}$ and $V^{(1)}_{e\ \text{term}}$ is performed with the standard techniques [7] but also verified with the new method.

Examples of the resulting matrix elements $\langle p', q', \alpha' | V^{(1)}_i | p, q, \alpha \rangle$ are given in Fig. 1 as a function of the momentum p. Here, we fix the momenta to be $p' = 0.268$ fm^{-1}, $q' = 2.842$ fm^{-1}, and $q = 0.132$ fm^{-1} and consider the following four channel combinations: $(\alpha' = \alpha = 1)$, $(\alpha' = 1, \alpha = 5)$, $(\alpha' = \alpha = 4)$, and $(\alpha' = 4, \alpha = 7)$. These channels correspond to the quantum numbers given in Table I. Channels $\alpha = 1$ and $\alpha = 5$ are especially important, as those two states provide the dominant components of the ^{3}H wave function. As can be noted, All three components of the N^{3}LO 3NF give a strong contribution: the $V^{(1)}_{\text{ring}}$ dominates for the channel combination $(\alpha' = \alpha = 1)$, $V^{(1)}_{2\pi\text{-}1\pi}$ for $(\alpha' = 1, \alpha = 5)$, and $V^{(1)}_{2\pi}$ for $(\alpha' = \alpha = 4)$ and $(\alpha' = 4, \alpha = 7)$. We emphasize, however, that the large size of these matrix elements (which contain certain admixtures of short-range operators) compared to the N^{2}LO terms does not necessarily imply that their effects in low-energy observables are large. The values of the LECs for $V^{(1)}_{d\ \text{term}}$ and $V^{(1)}_{e\ \text{term}}$ terms shown in Fig. 1 are set to be $c_D = 1$ and $c_E = 1$ in order to allow for a qualitative comparison of the strength of the individual terms. Their real contributions emerging after fitting the LECs c_D and c_E to experimental data are discussed in the next section. Figure 1 also clearly demonstrates that not all terms contribute to each channel combination owing to the spin-isospin dependence. The $V^{(1)}_{2\pi\text{-}1\pi}$ and $V^{(1)}_{d\ \text{term}}$ terms contribute to $V^{(1)}$ only to $(\alpha' = 1, \alpha = 5)$ and the $V^{(1)}_{e\ \text{term}}$ term contributes only to $(\alpha' = \alpha = 1)$. Further, $V^{(1)}_{\text{ring}}$ vanishes for $\alpha' = \alpha = 4$.

The component $V^{(1)}$ of V_{123} enters the dynamical equations for 3N bound and scattering states [29,30] (see below) only in combination with the permutation operator P forming the operator $V^{(1)}(1 + P)$. The permutation operator $P \equiv P_{12}P_{23} + P_{13}P_{23}$ is built from the transpositions P_{ij}, which interchange nucleons i and j. The aPWD scheme can be used to obtain the $V^{(1)}(1 + P)$ matrix elements directly [25], which allows us to avoid uncertainties associated with the partial-wave decomposition of the permutation operator. The resulting

TABLE I. Values of the discrete quantum numbers for selected α states, (3.1), with the total angular momentum $J = 1/2$, the total isospin $T = 1/2$, and its projection $M_T = -1/2$.

α	l	s	j	λ	I	t
1	0	0	0	0	$\frac{1}{2}$	1
4	1	0	1	1	$\frac{3}{2}$	0
5	0	1	1	0	$\frac{1}{2}$	0
7	2	1	1	0	$\frac{1}{2}$	0

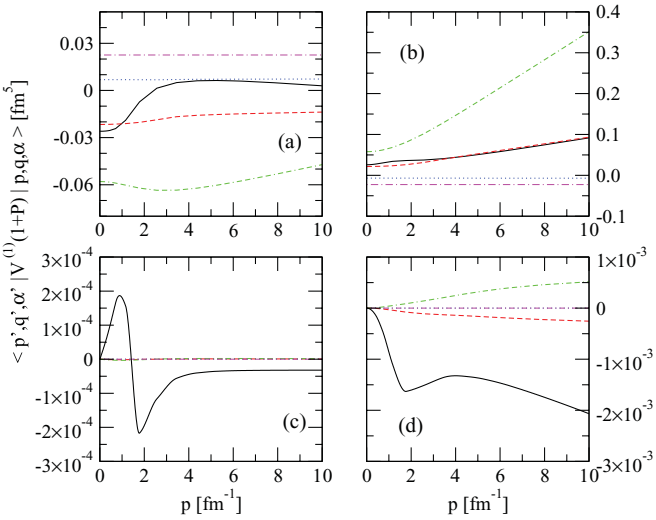

FIG. 2. (Color online) N^{3}LO 3NF matrix elements (before regularization) $\langle p', q', \alpha' | V^{(1)}(1+P) | p, q, \alpha \rangle$ as a function of the momentum p. The momenta p', q', and q, channel combinations (α', α), and lines are the same as in Fig. 1.

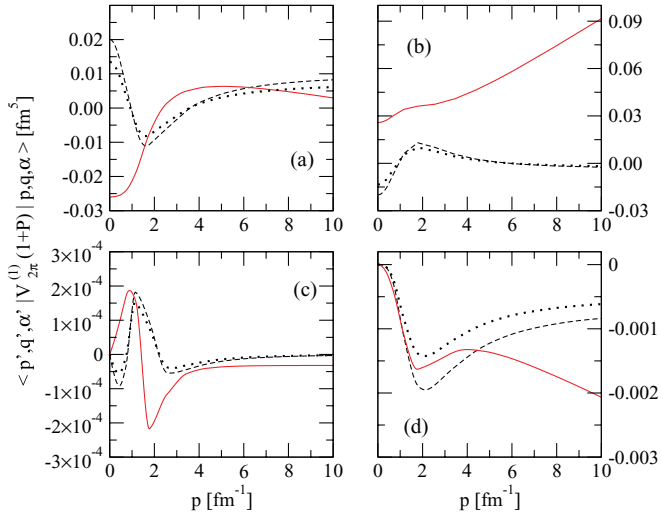

FIG. 3. (Color online) The 2π exchange part of 3NF matrix elements (before regularization) $\langle p', q', \alpha' | V^{(1)}_{2\pi}(1+P) | p, q, \alpha \rangle$ as a function of the p momentum. The momenta p', q', and q and channel combinations (α', α) are the same as in Fig. 1. Dashed (black) and solid (red) lines represent N^{2}LO and N^{3}LO results, respectively. The dotted (black) line describes the matrix elements of $V^{(1)}_{2\pi}(1+P)$ obtained with $\tilde{F}_1$ and $\tilde{F}_2$ artificially set to 0 (see text).

matrix elements $\langle p', q', \alpha' | V^{(1)}(1+P) | p, q, \alpha \rangle$ are given in Fig. 2 for the same momenta and channel combinations as in Fig. 1. Again, we observe that matrix elements of all contributions to the 3NF are large for these momenta. The $V^{(1)}_{\rm ring}$ contribution is particularly large in matrix elements with $\alpha' = 1$. For these channels also $V^{(1)}_{2\pi}$ and $V^{(1)}_{2\pi\text{-}1\pi}$ are significant. Moreover, for $\alpha' = \alpha = 1$ also $V^{(1)}_{d\ \rm term}$ and $V^{(1)}_{e\ \rm term}$ are non-negligible, at least with $c_D = 1$ and $c_E = 1$. For $\alpha' = 4$, the $V^{(1)}_{2\pi}$ piece dominates. Nevertheless, in the case of $\alpha = 7$ also $V^{(1)}_{\rm ring}$ provides a significant contribution. Owing to their spin-isospin structure, the $V^{(1)}_{d\ \rm term}$ and $V^{(1)}_{e\ \rm term}$ forces are absent for $(\alpha' = \alpha = 4)$ and $(\alpha' = 4, \alpha = 7)$ channel combinations.

The 2π exchange contribution at N^{3}LO can be compared with a corresponding part of the N^{2}LO interaction. An example is given in Fig. 3, where the dashed (solid) line represents the predictions obtained at N^{2}LO (N^{3}LO). The $V^{(1)}_{2\pi}(1+P)$ matrix elements differ significantly for all channel pairs considered. Figure 3 demonstrates that these differences mainly originate from the parts of the $V^{(1)}_{2\pi}$ interaction proportional to the $\tilde{F}_1$ and $\tilde{F}_2$ form factors [see Eqs. (2.4) and (2.5)]. In particular, in Fig. 3, we also show results for $V^{(1)}_{2\pi}(1+P)$ at N^{3}LO but with $\tilde{F}_1$ and $\tilde{F}_2$ artificially set to 0. In this case the only difference between matrix elements at N^{2}LO and N^{3}LO comes from the different values of c_i and $\tilde{c}_i$ LECs. The matrix elements presented, then, have a similar dependence on momentum p as well as a similar magnitude in N^{3}LO and N^{2}LO. Note, however, that these observations do not necessarily imply that the N^{3}LO corrections to the 3NF lead to large effects in low-energy three-nucleon observables. In fact, the opposite was observed in Ref. [22] for the case of the two-pion exchange topology.

The $V^{(1)}_i$ and $V^{(1)}_i(1+P)$ matrix elements shown in Figs. 1 and 2 have to be regularized prior to being used as input to the dynamical equations [7]. We use the regulator function of the form [1]

$$f(p,q) = \exp \frac{-(4p^2 + 3q^2)^3}{(4\Lambda^2)^3}, \tag{3.2}$$

which ensures that the large momenta are sufficiently suppressed. Following Ref. [1], we use three values of the Λ parameter: 450, 550, and 600 MeV. The regularization transforms matrix elements as

$$\langle p', q', \alpha' | V^{(1)}(1+P) | p, q, \alpha \rangle \rightarrow f(p', q') \langle p', q', \alpha' | V^{(1)}(1+P) | p, q, \alpha \rangle f(p, q). \tag{3.3}$$

The examples of the regularized $V^{(1)}(1+P)$ matrix elements are compared to the nonregularized ones in Fig. 4. This is done separately for $V^{(1)}_{2\pi}(1+P)$ and $V^{(1)}_{\rm ring}(1+P)$ contributions. The momenta are $p' = q' = q = 0.132$ fm^{-1} (upper row) and $p' = 0.268$ fm^{-1}, $q' = 2.842$ fm^{-1}, and $q = 0.132$ fm^{-1} (lower row) and we show only the $(\alpha' = \alpha = 1)$ channel combination. In the upper row, where the momenta p', q', and q are small, all regulator functions are close to 1 for small values of p. For momenta $p > 1$ fm^{-1}, the different Λ values lead to different slopes of matrix elements. The lowest value of the parameter $\Lambda = 450$ MeV forces the fastest decrease in $V^{(1)}_i(1+P)$ matrix elements. In this case, the short-range part of the interaction is suppressed. On the contrary, the highest value $\Lambda = 600$ MeV allows for larger contributions of short-range interactions. In the lower row in Fig. 4, where the momenta p' and q' are bigger, the effects of the regularization are seen already at low values of p. For $p = 0.001$ fm^{-1} the regularization factor $f(p', q') f(p, q)$ changes from 0.194 for $\Lambda = 450$ MeV to 0.747 for $\Lambda = 600$ MeV. This strong cutoff dependence is expected to be largely compensated by an appropriate "running" of the LECs c_D and c_E when calculating low-energy observables.

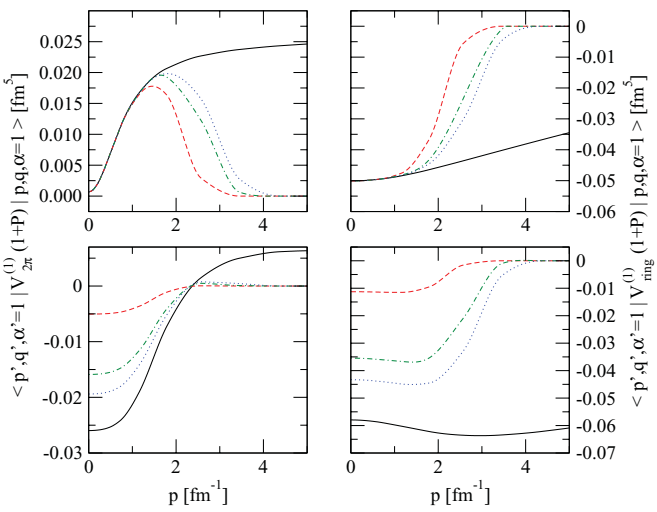

FIG. 4. (Color online) N^{3}LO 3NF matrix elements $\langle p', q', \alpha' = 1|V_i^{(1)}(1+P)|p, q, \alpha = 1\rangle$ as a function of the p momentum for the momenta $p' = q' = q = 0.132$ fm^{-1} (top) and $p' = 0.268$ fm^{-1}, $q' = 2.842$ fm^{-1}, and $q = 0.132$ fm^{-1} (bottom). The two components of the N^{3}LO 3NF are shown: $V_{2\pi}^{(1)}(1+P)$ (left) and $V_{\rm ring}^{(1)}(1+P)$ (right). The solid (black) line represents $V_{2\pi}^{(1)}(1+P)$ and $V_{\rm ring}^{(1)}(1+P)$ matrix elements before regularization. Dashed (red), dash-dotted (green), and dotted (blue) curves represent the $V_{2\pi}^{(1)}(1+P)$ and $V_{\rm ring}^{(1)}(1+P)$ matrix elements regularized as in Eq. (3.3) with $\Lambda =$ 450, 550, and 600 MeV, respectively.

IV. DETERMINATION OF LEC c_D AND c_E VALUES AT N^{3}LO

Once the new terms are added to the 3NF, the procedure for refitting the LECs c_D and c_E has to be repeated. We follow Ref. [7] and use the triton binding energy E^3H and the neutron-deuteron doublet scattering length $^2a_{nd}$ as two observables from which c_D and c_E can be obtained. The up-to-date experimental values are $E^3H = 8.481821(5)$ MeV [31] and $^2a_{nd} = 0.645(7)$ fm [32].

Our procedure to fix the values of LECs can be divided into two steps. First, the dependence of E^3H on c_E for a given value of c_D is determined. The requirement to reproduce the experimental value of the triton binding energy yields a set of combinations c_D and c_E. This set is then used in the calculations of $^2a_{nd}$, which allows us to find which pair of c_D and c_E describes both observables simultaneously. This procedure has to be repeated for all Λ values used in the regularization. The same values of the cutoff Λ are used to suppress high momenta in the NN potential in order to ensure the convergence of the integral in the Lippmann-Schwinger equation. The chiral NN potential depends, in addition, on another cutoff parameter, $\tilde{\Lambda}$, emerging from the SFR of the two-pion exchange potential. We follow Ref. [1] and use five combinations of $(\Lambda, \tilde{\Lambda})$ reported in Table II.

We compute the ^{3}H wave function using the method described in Ref. [30]. Here we mention only that the full triton wave function $\Psi = (1+P)\psi$ is given by its Faddeev component ψ, being the solution of the Faddeev equation:

$$\psi = G_0 t P \psi + (1 + G_0 t) G_0 V^{(1)}(1+P)\psi. \qquad (4.1)$$

TABLE II. Values of c_D and c_E LECs for different parametrizations of the chiral N^{3}LO potential.

Cutoff	$(\Lambda, \tilde{\Lambda})$	c_D	c_E
1	(450,500)	10.78	−0.172
2	(600,500)	12.00	1.254
3	(550,600)	11.67	2.120
4	(450,700)	7.21	−0.748
5	(600,700)	14.07	1.704

Here, G_0 is the free 3N propagator, P is the same permutation operator as defined above, and t is the two-body t operator generated from a given NN potential through the Lippmann-Schwinger equation.

We use the 3N states $|p, q, \alpha\rangle$ defined on the grids of 68 p points and 48 q points at intervals $p \in (0,\ 15)$ fm^{-1} and $q \in (0,\ 10)$ fm^{-1}, respectively. We take into account all states up to the two-body total angular momentum $j = 5$ for the NN potential and all states up to $j = 3$ for the 3N interaction.

We solve Eq. (4.1) and find pairs of the LECs c_D and c_E that reproduce the experimental value of E^3H. It is exemplified in the top panel in Fig. 5 for the third cutoff combination from Table II. The dependence is smooth, and for some values of c_E there are two possible values of c_D.

In the second step of the fitting procedure the doublet scattering length $^2a_{nd}$ is calculated for the (c_D, c_E) pairs, which reproduce the correct value of E^3H. With this aim, we first solve the Faddeev equation for the auxiliary amplitude T at

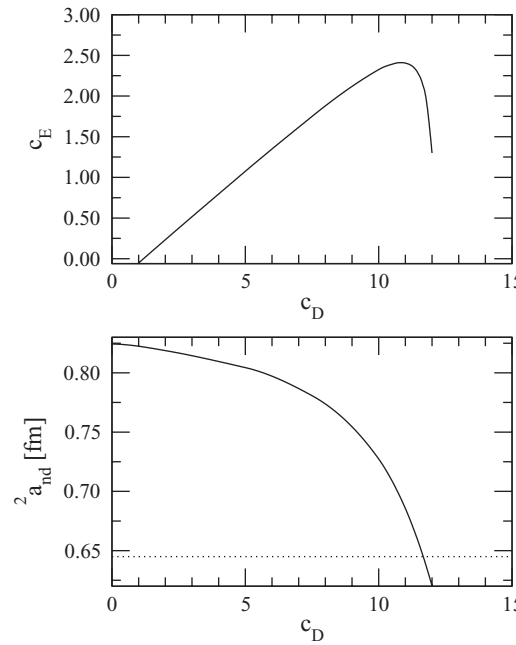

FIG. 5. (Color online) Intermediate results obtained during the fitting procedure for the c_D and c_E N^{3}LO LECs for the third cutoff combination from Table II: values of the c_D and c_E LECs that give the experimental E^3H (top) and the dependence of $^2a_{nd}$ on c_D (bottom). The dotted line shows the experimental value $^2a_{nd} = 0.645(7)$ fm [32].

zero incoming nucleon energy,

$$T = tP\phi + (1 + tG_0)V^{(1)}(1 + P)\phi + tPG_0T + (1 + tG_0)V^{(1)}(1 + P)G_0T, \quad (4.2)$$

where the initial channel state ϕ occurring in the driving terms is composed of the deuteron and a plane-wave state of the projectile nucleon. The amplitude for the elastic nucleon-deuteron scattering is then given by

$$U = PG_0^{-1} + PT + V^{(1)}(1 + P)\phi + V^{(1)}(1 + P)G_0T. \quad (4.3)$$

We refer to Refs. [29] and [33] for a general overview of 3N scattering and for more details on the practical implementation of the Faddeev equations. The expression for ${}^2a_{nd}$ in our basis and further technical details are given in Ref. [34]. In this second step of the fitting procedure we use grids of 32 p points in the range $p \in (0, 25)$ fm^{-1} and 31 q points in the range $q \in (0, 15)$ fm^{-1}. Similarly to the triton calculations, the NN (3N) potential acts in all states up to $j = 5(3)$. Our calculations are accurate up to 2 keV for the binding energy and up to 0.005 fm for the scattering length. We expect that, even in N^{3}LO, the chiral expansion of the nuclear forces induces uncertainties that are larger than these estimates. Therefore, the numerical calculations are sufficiently accurate to perform sensible fits of c_D and c_E at N^{3}LO.

The final values of c_D and c_E LECs, which reproduce the experimental values of $E^{^3H}$ and ${}^2a_{nd}$, are listed in Table II. For all combinations of cutoff parameters, the LEC c_D remains positive, with a value around 10. It weakly depends on the value of the cutoff Λ and becomes larger with increasing Λ. The second LEC, c_E, changes in a more complicated way. While again it is smallest in magnitude for the smallest value of Λ, its largest value is for the medium $\Lambda = 550$ MeV and then it decreases upon moving to $\Lambda = 600$ MeV. Note that c_E changes sign so the $V^{(1)}_{e\,\mathrm{term}}$ interaction changes from attractive to repulsive. We also stress that while the value of the LEC c_D appears to be rather large, the expectation value of the one-pion exchange-contact part of the 3NF is of a natural size. It remains to be seen whether the complete calculation including the remaining 3NF contributions at N^{3}LO will lead to more natural values of the LEC c_D.

Finally, we would like to emphasize that the values of the LECs that are *bare* parameters must be refitted at each order in the chiral expansion (and, of course, for each cutoff combination). This is in contrast with chiral perturbation theory calculations in the Goldstone-boson and single-nucleon sectors, where the scattering amplitude is usually expressed in terms of *renormalized* LECs. Indeed, using the values of c_D and c_E determined at N^{2}LO in the N^{3}LO calculation would generally result in a poor description of low-energy observables. For example, for the third cutoff combination, the 3NF at N^{3}LO furnished with the N^{2}LO values $c_D = -0.45$ and $c_E = -0.798$ [1] and combined with the N^{3}LO NN potential yields $E^{^3H} = -8.197$ MeV and ${}^2a_{nd} = 1.004$ fm, which are far from the experimental values. Similarly, while the combination $c_D = 1.5744$ and $c_E = -17.8$ allows us to reproduce the triton binding energy and the doublet nd scattering length for N^{3}LO NN force accompanied with the N^{2}LO 3NF, it produces $E^{^3H} = -7.542$ MeV and ${}^2a_{nd} = 1.4354$ fm when the N^{3}LO 3NF is used. Note that a large value of c_E obtained in this case seems to violate naturalness. These results demonstrate clearly that fitting to the data has to be made consistently within the given order of the chiral expansion. Therefore, also the results of our test fit here, which does not include the full 3NF at N^{3}LO, has to be taken with care. However, the fit results allow us to study the properties of ^{3}H in the next section.

V. THE PROPERTIES OF ^{3}H

Once the values of c_D and c_E low-energy parameters are established, one can explore the properties of the ^{3}H wave function. We begin with the expectation values of the kinetic energy $\langle H_0 \rangle$, the NN potential energy $\langle V_{NN} \rangle$, and the 3N potential energy $\langle V_{3N} \rangle$, which are listed in Table III. The expectation values clearly depend on the cutoff parameters Λ and $\tilde{\Lambda}$ as they should. Not surprisingly, the expectation values of both the NN potential and the 3NF are smallest for the softest cutoff $\Lambda = 450$ MeV. Higher Λ values lead to stronger 3NF contributions to the $E^{^3H}$, which, for $\Lambda = 600$ MeV, reaches about $\approx$20%. For all cutoff values, one clearly observes the dominance of the NN forces, $\langle V_{3N} \rangle / \langle V_{NN} \rangle = 1.5\% \cdots 3\%$, in agreement with the expectations based on the chiral power counting. Note that the interplay of N^{2}LO counter terms and N^{3}LO structures of the 3NF does not allow one to use these expectation values for an assessment of the contributions of N^{3}LO 3NFs. Similarly as in the NN interaction, one observes strong cancellations of N^{3}LO contributions also with N^{2}LO contact interactions. Such a comparison only makes sense for renormalized quantities, which we are not able to identify here. One also observes that the dependence of the expectation values on the SFR cutoff $\tilde{\Lambda}$ is less pronounced than the Λ dependence. For example, for cutoff combinations 1 and 4, which differ only in the choice of $\tilde{\Lambda}$, the $\langle H_0 \rangle$ and $\langle V_{NN} \rangle$ differ by about 3 MeV. On the other hand, the differences reach almost 20 MeV for the cutoff combinations 1 and 2, which have the same SFR cutoff $\tilde{\Lambda}$ but different values of Λ. This holds true also for $\langle V_{3N} \rangle$. In addition, we report in Table III the expectation values obtained with $\Lambda = 550$ MeV and $\tilde{\Lambda} = 600$ MeV but for N^{2}LO NN and 3N potentials. As a second example we give the same expectation values but

TABLE III. Expectation values $\langle H_0 \rangle$, $\langle V_{NN} \rangle$, and $\langle V_{3N} \rangle$ in the triton for different parametrizations of the chiral N^{3}LO potential discussed in the text. Parametrization denoted 3a (3b) shows results for Λ and $\tilde{\Lambda}$ as in cutoff 3 but for the N^{2}LO (N^{3}LO) NN potential combined with the N^{2}LO 3NF.

Cutoff	$\langle H_0 \rangle$ (MeV)	$\langle V_{NN} \rangle$ (MeV)	$\langle V_{3N} \rangle$ (MeV)
1	35.972	−43.459	−0.994
2	54.708	−61.515	−1.673
3	48.088	−55.187	−1.381
4	33.232	−41.050	−0.663
5	53.504	−60.278	−1.706
3a	33.174	−40.874	−0.770
3b	47.713	−54.650	−1.544

TABLE IV. Expectation values for the different parts of the 3N potential and for the different parametrizations of the chiral N^{3}LO potential.

Cutoff	$\langle V_{2\pi}\rangle$ (MeV)	$\langle V_{2\pi\text{-}1\pi}\rangle$ (MeV)	$\langle V_{\text{ring}}\rangle$ (MeV)	$\langle V_{d\ \text{term}}\rangle$ (MeV)	$\langle V_{e\ \text{term}}\rangle$ (MeV)
1	−0.639	0.458	−0.147	−0.693	0.027
2	−0.241	−0.580	−1.114	0.694	−0.432
3	−0.473	0.107	−0.191	−0.708	−0.116
4	−0.771	0.539	−0.452	−0.259	0.281
5	−0.377	−0.275	−0.622	−0.119	−0.313

obtained with the N^{3}LO NN potential combined with N^{2}LO3 NF. The values of LECs in both cases are chosen to reproduce the ^{3}H binding energy and are given above. As can be noted, for this cutoff, the size of $\langle V_{3N}\rangle$ depends on the order of the NN potential and does not vary significantly with the order of 3NF.

More detailed information about the 3NF triton expectation values is reported in Table IV. The expectation value of the 3NF $\langle V_{3N}\rangle$ is split into the individual contributions from various topologies. The expectation value of the two-pion exchange potential $\langle V_{2\pi}\rangle$ shows a smooth dependence on Λ. For the softest cutoff $\Lambda = 450$ MeV, the two-pion exchange 3NF turns out to be most attractive, providing more than 0.5 MeV to the triton binding energy. With increasing Λ, the contribution of $V_{2\pi}$ becomes weaker. For cutoff combination 2, $\Lambda = 600$ MeV, $\tilde{\Lambda} = 500$ MeV, the additional binding owing to the two-pion exchange 3NF only amounts to about 240 keV. Interestingly, most of the attraction necessary to reproduce the triton binding energy is produced in this case by the ring topology, which is found to be attractive for all cutoff combinations. Contrary to the longest range two-pion exchange topology, the contributions of the ring diagrams are enhanced for the largest value of the cutoff $\Lambda = 600$ MeV. Qualitatively, this behavior might be expected given the fact that the large values of Λ probe the shorter range part of V_{ring}, which is of the van der Waals type; i.e., the matrix elements grow rapidly with decreasing relative distances between the nucleons. The cutoff dependence of this contribution is very large. This explicitly shows the dependence on the short-distance pieces, making it impossible to estimate the impact of this topology on low-energy observables based on our results. The expectation value of the two-pion/one-pion exchange topology $\langle V_{2\pi\text{-}1\pi}\rangle$ also strongly depends on Λ. It changes sign from positive for $\Lambda = 450$ MeV to negative at $\Lambda = 600$ MeV. The dependence on the SFR cutoff is fairly weak. Note, however, that a stronger dependence might be induced once the SFR regularized $A(q)$ has been taken into account. The $\langle V_{d\ \text{term}}\rangle$ shows the most complicated behavior. It achieves the lowest value for the intermediate value of Λ (cutoff combination 3) and, for $\Lambda = 600$ MeV, shows a strong dependence on the SFR cutoff $\tilde{\Lambda}$. In particular, for the smaller value $\tilde{\Lambda} = 500$ MeV, this contribution to the 3NF becomes repulsive and relatively large, while for $\tilde{\Lambda} = 700$ MeV the expectation value remains negative. Finally, the $\langle V_{e\ \text{term}}\rangle$ expectation value changes smoothly with Λ. It also changes its sign from positive at the lowest Λ to negative at $\Lambda = 600$ MeV. Last but not least, we emphasize that the expectation values discussed above as well as the separation of the potential energy into the contributions owing to the NN potential and 3NF do *not* correspond to observable quantities and are expected to show a strong cutoff dependence. Notice, further, that expectation values of the various 3NF contributions are, strictly speaking, bare quantities. Comparing their size with that of the N^{2}LO terms, therefore, does not allow one to draw conclusions about the convergence of the chiral expansion [39]. It is comforting to see that all expectation values turn out to be of a reasonable size.

We now turn to the two-nucleon correlation function of ^{3}H, which is defined as [30]

$$C(r) \equiv \frac{1}{3}\frac{1}{4\pi}\int d\hat{r}\langle\Psi|\sum_{i<j}\delta(\vec{r}-\vec{r}_{ij})|\Psi\rangle\,. \qquad (5.1)$$

Here, $\vec{r}_{ij}$ is the relative distance corresponding to the Jacobi momentum $\vec{p}$. In Fig. 6 the correlation function is shown for the same combinations of the regularization parameters as in Table II. Thin lines represent predictions based on NN interactions only, while thick lines show the predictions based on NN + 3N forces. As expected, the softest cutoff value $\Lambda = 450$ MeV yields a flatter correlation function the less the amount of short-range correlations. The higher Λ values prefer distributions concentrated around the maximum at $r \approx 1.5$ fm. The effects of the 3NFs are small for the lowest Λ but increase with increasing Λ. For the lowest Λ there is also a strong dependence of the correlation function on the SFR parameter $\tilde{\Lambda}$.

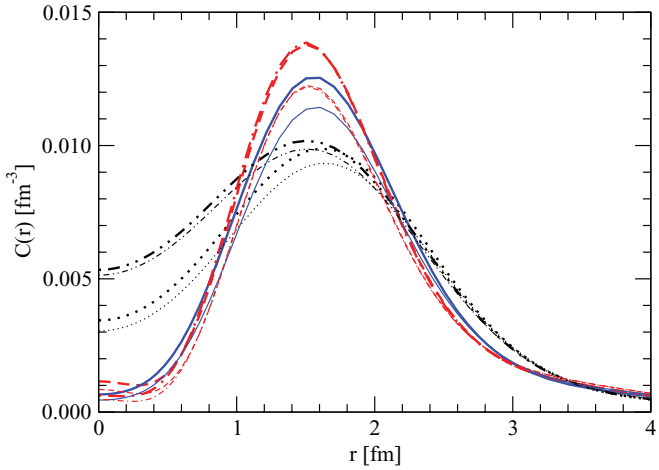

FIG. 6. (Color online) Two-body correlation function for the triton for different $(\Lambda, \tilde{\Lambda})$ pairs listed in Table II. The thin dotted (black), dashed (red), solid (blue), dash-double-dotted (black), and dash-dotted (red) lines correspond to predictions based only on the NN interaction with cutoff numbers from 1 to 5, respectively. The thick lines represent predictions with the same regularization parameters but based on NN and 3N forces.

VI. SUMMARY AND OUTLOOK

In this paper we, for the first time, have included the long-range N^{3}LO corrections to the 3NF in the Faddeev calculations. These novel two-pion exchange, two-pion/one-pion, and ring interactions supplemented with the one-pion exchange and contact terms emerging at N^{2}LO represent, presently, the most advanced chiral 3NF. We use this force in the triton and the doublet neutron-deuteron scattering length Faddeev calculations to fix the two low-energy parameters c_D and c_E for different sets of regularization parameters, which cut off high-momentum or, equivalently, short-range components in few-nucleon states. While the value of the LEC c_D remains fairly stable, c_E features a stronger sensitivity to regularization parameters. It will be interesting whether such a behavior is also seen for fits involving the complete N^{3}LO 3NF. We also studied the individual contributions of the various topologies to the triton binding energy. The expectation values of the two-pion/one-pion and ring terms turn out to be smaller than the ones of the dominant two-pion exchange 3NF for softer values of the regulator. Generally, all expectation values are found to be sizable. As expected, we observe a strong sensitivity of the expectation values to the regularization parameters. We also looked at the impact of the 3NF used on the two-nucleon correlation function in the triton.

While our work does not yet correspond to a complete N^{3}LO analysis, owing to the shorter range contributions and relativistic corrections to the 3NF that are not yet available and are still missing in our calculations, it does represent a very important step in this direction and provides a proof-of-principle that the very complex operator structure of the 3NF at N^{3}LO can be successfully implemented in few-body calculations. In the future, this study should be extended to explore effects of the novel terms in the 3NF in few-nucleon scattering. This work is in progress. To complete the analysis of the 3NF at N^{3}LO the inclusion of the full structure of shorter range $V^{(1)}_{1\pi\ \mathrm{cont}}$, $V^{(1)}_{2\pi\ \mathrm{cont}}$, and $V^{(1)}_{1/m}$ terms should be pursued. The numerical implementation of the new terms can be straightforwardly performed using the newly developed aPWD scheme, which is successfully tested for the long-range terms in the present study. Even more interesting will be the study of the 3NF at N^{4}LO, which is expected to be significant. This expectation is discussed in Ref. [3] and, additionally, guided by recent results from the Δ-full chiral perturbation theory [35]. Of course, also at N^{4}LO the aPWD method can be used for numerical implementation of the 3NF. Finally, it should be emphasized that the present work also opens the way to applying the novel chiral nuclear forces in many-body calculations (see, e.g., Refs. [36–38] for some exciting recent developments along these lines based on N^{2}LO 3NFs).

ACKNOWLEDGMENTS

This work was supported by the Polish Ministry of Science and Higher Education under Grant No. N N202 077435. It was also partially supported by the Helmholtz Association (Grant Nos. VH-NG-222 and VH-VI-231), by the European Community-Research Infrastructure Integrating Activity "Study of Strongly Interacting Matter" (HadronPhysics2; Grant Agreement No. 227431) under the Seventh Framework Programme of the European Union and the European Research Council (ERC-2010-StG 259218 NuclearEFT). We also acknowledge support by the Foundation for Polish Science–MPD program, cofinanced by the European Union within the European Regional Development Fund. The numerical calculations were performed on the supercomputer cluster at the JSC, Jülich, Germany, and ACK-Cyfronet, Kraków, Poland.

[1] E. Epelbaum, Prog. Part. Nucl. Phys. **57**, 654 (2006).
[2] E. Epelbaum, H.-W. Hammer, and Ulf-G. Meißner, Rev. Mod. Phys. **81**, 1773 (2009).
[3] R. Machleidt and D. R. Entem, Phys. Rep. **503**, 1 (2011).
[4] E. Epelbaum, W. Glöckle, and U.-G. Meißner, Nucl. Phys. A **747**, 362 (2005).
[5] D. R. Entem and R. Machleidt, Phys. Rev. C **68**, 041001 (2003).
[6] E. Epelbaum, W. Glöckle, and U.-G. Meißner, Eur. Phys. J. A **19**, 125 (2004).
[7] E. Epelbaum, A. Nogga, W. Glöckle, H. Kamada, U.-G. Meißner, and H. Witała, Phys. Rev. C **66**, 064001 (2002).
[8] U. van Kolck, Phys. Rev. C **49**, 2932 (1994).
[9] E. Epelbaum, H. Krebs, D. Lee, and U.-G. Meißner, Eur. Phys. J. A **41**, 125 (2009).
[10] A. Nogga, P. Navratil, B. R. Barrett, and J. P. Vary, Phys. Rev. C **73**, 064002 (2006).
[11] E. Epelbaum, H. Krebs, D. Lee, and U.-G. Meißner, Phys. Rev. Lett. **106**, 192501 (2011).
[12] P. Navratil, V. G. Gueorguiev, J. P. Vary, W. E. Ormand, and A. Nogga, Phys. Rev. Lett. **99**, 042501 (2007).
[13] D. Gazit, S. Quaglioni, and P. Navratil, Phys. Rev. Lett. **103**, 102502 (2009).
[14] St. Kistryn *et al.*, Phys. Rev. C **72**, 044006 (2005).
[15] N. Kalantar-Nayestanaki and E. Epelbaum, Nucl. Phys. News. **17**, 22 (2007).
[16] R. B. Wiringa, V. G. J. Stoks, and R. Schiavilla, Phys. Rev. C **51**, 38 (1995).
[17] B. S. Pudliner, V. R. Pandharipande, J. Carlson, Steven C. Pieper, and R. B. Wiringa, Phys. Rev. C **56**, 1720 (1997).
[18] R. Machleidt, F. Sammarruca, and Y. Song, Phys. Rev. C **53**, R1483 (1996).
[19] S. A. Coon *et al.*, Nucl. Phys. A **317**, 242 (1979); S. A. Coon and W. Glöckle, Phys. Rev. C **23**, 1790 (1981).
[20] H. Witała *et al.*, Phys. Rev. C **63**, 024007 (2001).
[21] J. L. Friar and S. A. Coon, Phys. Rev. C **49**, 1272 (1994).
[22] S. Ishikawa and M. R. Robilotta, Phys. Rev. C **76**, 014006 (2007).
[23] V. Bernard, E. Epelbaum, H. Krebs, and U.-G. Meißner, Phys. Rev. C **77**, 064004 (2008).
[24] J. Golak *et al.*, Eur. Phys. J. A **43**, 241 (2010).
[25] R. Skibiński *et al.*, Eur. Phys. J. A **47**, 48 (2011).

[26] V. Bernard, E. Epelbaum, H. Krebs, and U.-G. Meißner, Phys. Rev. C **84**, 054001 (2011).
[27] P. Büttiker and U.-G. Meißner, Nucl. Phys. A **668**, 97 (2000).
[28] W. Glöckle, *The Quantum Mechanical Few-Body Problem* (Springer-Verlag, Berlin, 1983).
[29] W. Glöckle, H. Witała, D. Hüber, H. Kamada, and J. Golak, Phys. Rep. **274**, 107 (1996).
[30] A. Nogga, D. Hüber, H. Kamada, and W. Glöckle, Phys. Lett. B **409**, 19 (1997).
[31] G. Audi and A. H. Wapstra, Nucl. Phys. A **595**, 409 (1995), and references therein.
[32] K. Schoen *et al*., Phys. Rev. C **67**, 044005 (2003).
[33] D. Hüber, H. Kamada, H. Witała, and W. Glöckle, Acta Phys. Polon. B **28**, 1677 (1997).
[34] H. Witała *et al*., Phys. Rev. C **68**, 034002 (2003).
[35] H. Krebs and E. Epelbaum, Few-Body Syst. **50**, 295 (2011).
[36] P. Navratil, S. Quaglioni, I. Stetcu, and B. R. Barrett, J. Phys. G **36**, 083101 (2009).
[37] R. Roth, J. Langhammer, A. Calci, S. Binder, and P. Navratil, Phys. Rev. Lett. **107**, 072501 (2011).
[38] T. Lesinski, K. Hebeler, T. Duguet, and A. Schwenk, arXiv:1104.2955 [nucl-th].
[39] In fact, r-space potentials generated by the long-range N^3LO contributions are much weaker than those emerging from the leading two-pion exchange terms at relative distances of the order of the inverse pion mass.